

Three-Dimensional Grain Boundary Spectroscopy in Transparent High Power Ceramic Laser Materials

Mariola O. Ramirez^{1*}, Jeffrey Wisdom², Haifeng Li³, Yan Lin Aung⁴, Joseph Stitt¹, Gary L. Messing¹, V. Dierolf⁵, Zhiwen Liu³, Akio Ikesue⁴, Robert L. Byer² and Venkatraman Gopalan¹

¹Department of Materials Science and Engineering and Materials Research Institute, Pennsylvania State University, University Park, PA 16802

²Department of Applied Physics, Ginzton Laboratory, Stanford University, Palo Alto, CA 94304

³Department of Electrical Engineering, Pennsylvania State University, University Park, PA 16802

⁴World-Lab Co., Ltd., Atsuta-ku, Nagoya 456-0023, Japan

⁵Department of Physics, 16 Memorial Drive, Bethlehem, PA 18015, USA

*Corresponding author: mdr20@psu.edu

Abstract: Using confocal Raman and fluorescence spectroscopic imaging in 3-dimensions, we show direct evidence for Nd³⁺-Nd³⁺ interactions across grain boundaries (GBs) in Nd³⁺:YAG laser ceramics. It is clearly shown that Nd³⁺ segregation takes place at GBs leading to self-fluorescence quenching which affects a volume fraction as high as 20%. In addition, we show a clear trend of increasing spatial inhomogeneities in Nd³⁺ concentration when the doping levels exceeds 3 at%, which is not detected by standard spectrometry techniques. These results could point the way to further improvements in what is already an impressive class of ceramic laser materials.

©2007 Optical Society of America

OCIS codes: (140.3390) Laser materials processing. (140.5680) Rare earth and transition metal solid-state lasers. (180.6900) Three-dimensional microscopy. (300.6360) Spectroscopy, laser.

References and links

1. A. Ikesue, Y.L. Aung, T. Taira, T. Kamimura, K. Yoshida and G.L. Messing, "Progress in Ceramic Lasers," *Ann. Rev. Mater. Res.* **36**, 397-429 (2006).
2. A. Ikesue, and Y.L. Aung, "Synthesis and Performance of Advanced Ceramic Lasers," *J. Am. Ceram. Soc.* **89**, 1936-1944 (2006).
3. J. Wisdom, M. Dignonnet and R.L. Byer, "Ceramic Lasers: Ready for Action," *Photonic Spectra* **38**, 2-8 (2004).
4. G.A. Kumar, J. Lu, A.A. Kaminskii, K. Ueda, H. Yagi, T. Yanagitani and N.V. Unnikrishnan "Spectroscopic and Stimulated Emission Characteristics of Nd³⁺ in Transparent YAG Ceramics," *IEEE J. Quantum Electron.* **40**, 747-758 (2004).
5. V. Lupei, N. Pavel, and T. Taira, "1064 nm laser emission of highly doped Nd :Yttrium aluminum garnet under 885 nm diode laser pumping," *Appl. Phys. Lett.* **80**, 4309-4312, (2002).
6. A. Ikesue, K. Kamata, and K. Yoshida, "Effects of Neodymium Concentration on Optical Characteristics of Polycrystalline Nd:YAG Laser Materials," *J. Am. Ceram. Soc.* **79**, 1921-1926 (1996).
7. R. Kawai, Y. Miyasaka, K. Otsuka, T. Ohtomo and T. Narita, "Oscillation spectra and dynamics effects in highly-doped microchip Nd :YAG ceramic laser," *Opt. Express*, **12**, 2293-2302 (2004).
8. K. Otsuka, T. Narita, Y. Miyasaka, C. Lin and J. Ko, "Nonlinear dynamics in thin-slice Nd :YAG ceramic lasers : Coupled local-mode laser model," *Appl. Phys. Lett.* **89**, 081117 (2006).
9. T. Sekino, and Y. Sogabe, "Progress in the YAG Crystal Growth Technique for Solid State Lasers," *Rev. Laser Eng.* **21**, 827-831 (1995).
10. A. Ikesue, T. Kinoshita, K. Kamata, and K. Yoshida, "Fabrication and Optical Properties of High-Performance Polycrystalline Nd:YAG Ceramics for Solid-State Lasers," *J. Am. Ceram. Soc.* **78**, 1033-1040 (1995).

11. T. Taira, "RE³⁺ ion-doped YAG ceramic lasers," *IEEE J. Select Topcs Quantum Electron.* **13**, 789-809 (2007).
12. T. Taira, "Ceramic YAG lasers," *Comptes Rendus Phys.* **8**, 138-152 (2007).
13. S.H. Lee, S. Kochawattana, G.L. Messing, J. Q. Dumm, G. Quarles and V. Castillo, "Solid-state reactive sintering of transparent polycrystalline Nd:YAG ceramic," *J.Am. Ceram. Soc.* **89**, 1945-1950 (2006).
14. A. Ikesue and K. Yoshida, "Scattering in Polycrystalline Nd :YAG Lasers," *J.Am. Ceram. Soc.* **81**, 2194-2196 (1998).
15. S. Geller, L.D. Fullmer, P.B. Crandall and G.P. Espinosa, "Thermal-expansion of some garnets," *Mater. Res. Bull.* **7**, 1219-1224 (1972).
16. J.P.Hurrell, S.P. Porto, I.F. Chang, S.S. Mitra and R.P. Bauman, "Optical Phonons of Yttrium Aluminum Garnet," *Phys. Rev* **173**, 851-856 (1968).
17. K. Papagelis, G. Kanellis, S. Ves. And G.A. Kourouklis, "Lattice Dynamical Properties of the Rare Earth Aluminum Garnets (RE₃Al₅O₁₂)," *Phys. Stat. Sol (b)* **233**, 134-150 (2002).
18. Y.F. Chen, P.K. Lim, S.J. Lim, Y.J. Yang, L.J. Hu, H.P. Chiang and W.S. Tse, "Raman scattering investigation of Yb :YAG crystals grown by the Czochralski method," *J. Raman Spectrosc.* **34**, 882-885 (2003).
19. V. Lupei, A. Lupei, S. Georgescu, T. Taira, Y. Sato and A. Ikesue, "The effect of Nd concentration on the spectroscopic and emission decay properties of highly doped Nd :YAG ceramics," *Phys. Rev. B* **64**, 092102 (2001).
20. V. Lupei, A. Lupei, S. Georgescu, T. Taira, Y. Sato, S. Kurimira and A. Ikesue "High-resolution spectroscopy and emission decay in concentrated Nd :YAG ceramics," *J. Opt. Soc. Am. B* **19**, 360-368 (2002).
21. V. Lupei, A. Lupei, and A. Ikesue, "Single crystal and transparent ceramic Nd-doped oxide laser materials : a comparative spectroscopic investigation," *J. Alloys Compd.* **380**, 61-70 (2004).
22. U.Aschauer and P. Bowen, "Atomistic Modeling Study of Surface Segregation in Nd :YAG," *J.Am. Ceram. Soc.* **89**, 3812-3816 (2006).
23. J.W. Cahn, "The impurity drag effect in grain boundary motion," *Acta Met.* **10** 789-798 (1962).
24. S. F. Akhmetov, G. L. Akhmetova, G. A. Gazizova, V. S. Kovalenko, and T. F. Mirenkova, "Rare earth metal aluminum garnets," *Russ. J. Inorg. Chem.*, **22**, 1613-1615, (1977).
25. A.E. Siegman, "Effects of Small-scale phase perturbations on laser oscillator beam quality," *IEEE J. Quantum Electron.* **17**, 334-337 (1977).
26. W.P. Risk, "Modeling of longitudinally pumped solid-state lasers exhibiting reabsorption losses," *J. Opt. Soc. Am. B* **5**, 1412-1423 (1988).

1. Introduction

The recent development of transparent ceramic laser materials with dense grain boundaries and performance exceeding single crystals is a paradigm shift in the field of laser materials. With solid state processing, it is now possible to achieve an order of magnitude increase in the concentration of active ions over single crystals, window-pane size laser materials, and engineered dopant profiles otherwise not possible in single crystal growth [1-3]. Of particular relevance here is the case of Nd³⁺:YAG ceramics where power scaling up to the kilowatt-level has been demonstrated [4]. On the other hand, the theoretical performance should be even higher; instead a decrease in the laser slope efficiency, a degradation of the beam quality factor and several dynamic instabilities are seen with increased doping, the atomistic and microscopic origin of which are presently not understood [5-8].

Nd³⁺ doped yttrium aluminum garnet; Y₃Al₅O₁₂ (YAG), is currently the most widely employed solid-state laser material for micromachining, medical operations, materials processing and many other industrial and defense applications. Nd³⁺:YAG lasers are based on single crystals, that are restricted to a maximum concentration of 1.4 at. % Nd³⁺, as well as to centimeters in dimensions [9]. This relatively low concentration level leads to a moderate Nd³⁺ pump absorption, strongly limiting the development of lasers of compact size, high power and efficiency. In 1995, Ikesue *et al.* was the first to demonstrate efficient laser action in transparent *polycrystalline* Nd³⁺:YAG with equal or superior optical quality to conventional laser single crystals [10]. Furthermore, up to 9 at.% Nd³⁺ doped YAG ceramics were achieved without any deterioration in the achievable sample size or the optical quality. Since then, because of the significant potential for a new era of laser materials that are *not* single crystals,

in addition to the obvious advantages in scaling, processing speed and cost, ceramic lasers gain media has become a highly active area of research worldwide [1,3,11-13].

Despite the extraordinarily rapid progress achieved in transparent laser ceramics, it appears they could be even better! Many open questions remain: How do grain boundaries (GBs) affect the optical response of laser active ions in ceramics? Why is there a variation in the laser performance between samples that are otherwise identical in scattering and doping levels?[14] How are laser slope efficiency, beam quality, and mode stability influenced by grain boundaries? [2,7,8] Otsuka *et al.* postulate the possible presence of saturable absorber-type defects in the GB, but no direct evidence for it exists [8]. Using 3-dimensional confocal Raman and fluorescence spectroscopy, we show evidence for Nd³⁺-segregation at the grain boundaries, subsequent fluorescence quenching and extensive spatial inhomogeneity in dopant concentration, that can explain many of the observed performance behaviors.

2. Materials and methods

Materials synthesis: Neodymium doped yttrium-aluminum garnet (Y₃Al₅O₁₂, Nd³⁺:YAG) transparent ceramics with Nd³⁺ concentrations ranging from 1-5.5 a.% exhibiting nearly the same optical properties as those of a single crystal were fabricated by a solid-state reaction method using high purity powders. High purity Y₂O₃, Al₂O₃ and Nd₂O₃ powders (99.99~99.999% purity) were used as starting materials. These powders were blended with the stoichiometric ratio of YAG including Nd³⁺ of 1.0, 2.3, 3.5, and 5.2 at% and ball milled for 12 h in ethanol with 0.5mass% TEOS (tetraethyl orthosilicate) added as a sintering aid. Then the alcohol solvent was removed by spray drying the milled slurry. Spherical granules (ca. 30~50 μm) having a homogeneous composition were obtained. The spray dried powder was pressed with low pressure into required shapes in a metal mold and then cold isostatically pressed at 98~196 MPa. Transparent Nd³⁺:YAG ceramics were obtained after sintering under vacuum (1x10⁻³Pa) at 1750°C for 10 hours. Unlike single crystal growth, solid state sintering up to 9 at% Nd³⁺, which is near to 12% solubility for Nd³⁺ ions in YAG, yields homogeneous Nd³⁺ doping without macroscopic gradients. For our studies, all the samples were unetched and surfaces polished to laser quality. No grain boundaries were observable under optical microscope or atomic force microscope.

Confocal Imaging: For confocal spectroscopic characterization, room temperature Raman and Fluorescence spectra were recorded by a WITec alpha300 S device using both tunable Argon and He-Ne lasers coupled into a single mode optical fiber. The signal was collected in backscattering geometry with the same objective (100 x magnification, numerical aperture, N.A = 0.9 in air) and focused into a multi-mode fiber (50 μm) that acts as pinhole for confocal microscopy. For the 514 nm excitation wavelength, the laser was focused to a diffraction-limited spot size of about 355 nm. In the axial direction, a conservative estimate of resolution is $2\lambda n/(N.A)^2 = 1270$ nm in air, and approximately 700 nm inside YAG (where $n=1.84$ for YAG (3) and $N.A=1.84 \times 0.9$ inside YAG). In order to evaluate the influence of far field contribution to fluorescence, experimental measurements of the doping profile was performed on a junction of a 1 at % doped Nd³⁺:YAG with an undoped single crystal YAG fabricated by diffusion bonding. The resulting measured doping profile shows that the concentration change at the interface (10-90% change) occurs over 800nm, which indicates the 10-90% lateral resolution of the fluorescence imaging in detecting interfaces. Thus, the ~2μm FWHM (25% to 75% change) in fluorescence signal across the grain boundary in Fig 2(d) is well resolved. The far-field contribution was below 10% signal level, observed as a weak “tail” in the fluorescence over 4-5μm. Therefore, for the average grain sizes studied in this work, the far-field contribution is small and can be neglected.

3. Results and discussion

The crystal structure of YAG materials belongs to the space group $Ia3d(O_h^{10})$. It contains eight molecular units in the unit cell. Three different sites are available in the lattice. The dodecahedral site c with local symmetry D_2 , is normally occupied by the large Y^{3+} ions surrounded by eight O^{2-} ions, the octahedral site a (local symmetry C_{3i}) is normally occupied by Al^{3+} surrounded by six O^{2-} ions and the tetrahedral site d (local symmetry S_4) is occupied by Al^{3+} . The Al^{3+} cations occupy eight octahedral sites of C_{3i} symmetry and twelve tetrahedral sites of S_4 symmetry. Nd^{3+} ions usually replace Y^{3+} cations placed in twelve dodecahedral sites of D_2 symmetry[15]. The large number of atoms in the primitive cell leads to 240 (3×80) possible normal modes which can be classified according to the irreducible representation of the O_h group as follows:

$$\Gamma = 18T_{1u} + 3A_{1g} + 8E_g + 14T_{2g} + 5A_{2g} + 5A_{1u} + 5A_{2u} + 10E_u + 14T_{1g} + 16T_{2u} \quad (1)$$

The 25 modes having symmetries A_{1g} , E_g and T_{2g} are Raman active while the 18 having T_{1u} symmetry are IR active. 23 of the 25 Raman active vibrational modes can be observed in the Raman spectrum from 0 to 900 cm^{-1} . The Raman spectrum of rare earth doped YAG compounds can be divided into two different parts: the high frequency region (500-900 cm^{-1}) and the low frequency region (<500 cm^{-1}). The high frequency region accounts to the ν_1 (breathing mode), ν_2 (quadrupolar) and ν_4 molecular internal modes associated with the (AlO_4) group, whilst the low frequency region is due to: (i) translational motion of the rare earth ions, (ii) rotational and translational motion of the AlO_4 units, and (iii) the ν_3 molecular mode of the AlO_4 [16-18]. Since the main goal of our work concerns the state of doping ions in ceramic materials in the vicinity of GBs, we have focused our attention on the low frequency region.

The optically transparent Nd^{3+} :YAG samples with Nd^{3+} doping of 1, 2.3, 3.5, and 5.2% at% were prepared by Ikesue *et al.* using solid-state reaction sintering (methods section). We first focus on the 1 at% doped sample. Fig. 1A shows three different Raman spectra in the low frequency region corresponding to three distinct grains in the sample. The relative intensities of the E_g and T_{2g} modes are strongly modified depending on the analyzed grain. On the contrary, the intensity of the A_{1g} lattice symmetric mode peaking at ~ 370 cm^{-1} remains constant regardless the examined grain. This behavior can be explained in terms of the randomly oriented nature of micro-crystals in polycrystalline ceramics and the Raman scattering intensity calculated from the scattering matrices (M) [16], which predict no intensity change with orientation for the A_{1g} lattice symmetric modes, and changes for the rest. We also do not see any changes for the A_{1g} mode in the region of the grain boundaries. This indicates that no excessive strain is present in these regions. We utilize this property to generate a total *spectroscopic* image of the grain pattern in the sample (Fig. 1B). The changes in Raman intensity for the E_g and T_{2g} modes can be exploited in a variety of ways to visualize the different grains. For instance, a clear distinction between different grains is achieved when

the center of mass, defined as $CM = \frac{\sum_{i=1}^n x_i I_i}{\sum_{i=1}^n I_i}$, is calculated in the spectral region 360-

405 cm^{-1} , which changes from grain to grain because A_{1g} mode is constant while the E_g is changed. Fig. 1C shows a different view of the same scanned area obtained by analyzing the integrated intensity of T_{2g} mode at 263 cm^{-1} . As observed, not only differences between the grains are observed but also a clear contrast between grains and GBs is manifested. No evidence of GBs was observed in undoped YAG ceramics. Fig.1D shows the evolution of this Raman peak as a function of Nd^{3+} concentration. As the Nd^{3+} content increases, a clear asymmetric broadening and a slight shift to lower wavenumbers is observed, because of the translatory motion of Nd^{3+} ions in combination with the heavy mixing of the translational, rotational and ν_3 mode of the (AlO_4) unit. Similar results were obtained for all the Raman modes in the low frequency region. Although the intensity effect observed in Fig.1C is mainly dominated by the orientation of the grains, the obtained contrast at GBs was not observed for

the Raman modes in the high frequency region, and hence can be tentatively assigned to different Nd³⁺ distribution between grains and GBs.

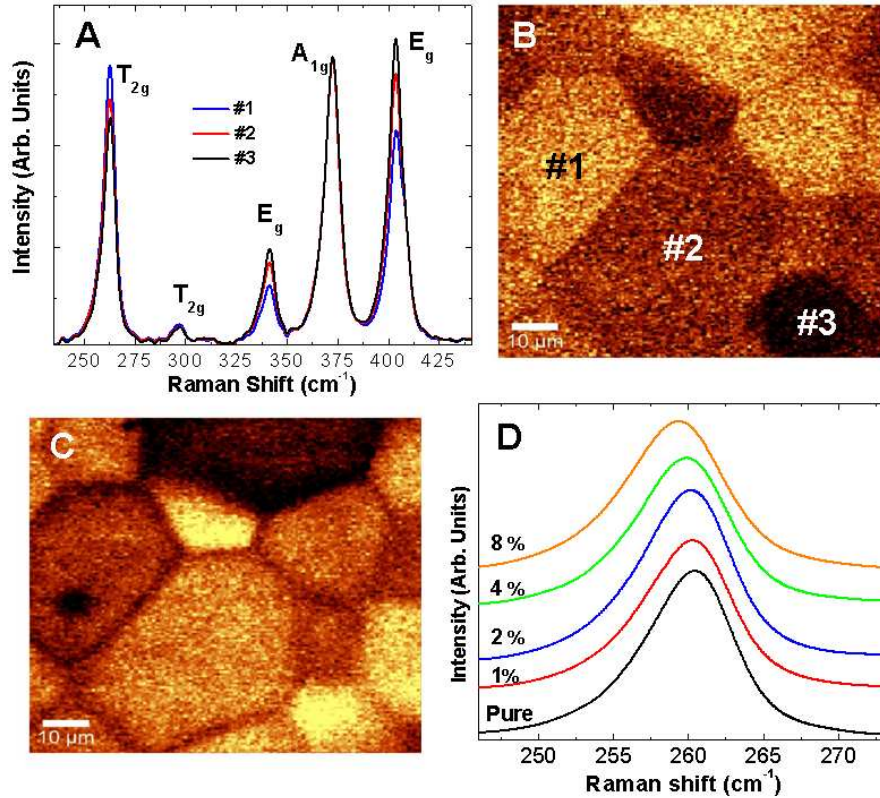


Fig. 1 (A) Detail of the Room Temperature (RT) Raman spectra recorded in confocal geometry at a depth of 10 μm below the surface at three different spatial regions in a transparent 1 at% Nd³⁺ doped YAG ceramic. The excitation wavelength was 488 nm. The symmetry of the different Raman modes has also been included for the sake of clarity. (B) Lateral Raman image (x - y scan; 85 x 85 μm) obtained in confocal geometry at a depth of 10 μm below the surface when the center of mass was fixed in the spectral region 360-405 cm^{-1} . Note that at every pixel in the Raman image, an entire Raman spectrum was collected (C) Lateral Raman image (x - y scan; 85 x 85 μm) obtained by integrating over the 243-273 cm^{-1} spectral region. The scanned area is the same as (B). (D) Raman shift of the T_{2g} mode as a function of Nd³⁺ concentration.

To gain further insight into the Nd³⁺ distribution and activity across a GB, two types of confocal fluorescence experiments were performed: Lateral imaging and Depth Imaging. For the cubic symmetry of the host material and in the absence of excessive stress (as concluded from Raman), a uniform intensity distribution is expected from grain to grain and in the grain boundaries unless variation in Nd³⁺ concentrations and emission quantum efficiency are present. Figure 2A shows the three dimensional (x and y positions versus intensity) fluorescence image obtained in the lateral geometry by integrating over the whole emission area corresponding to the ${}^4F_{7/2} : {}^4S_{3/2} \rightarrow {}^4I_{9/2}$ and ${}^4F_{3/2} \rightarrow {}^4I_{9/2}$ electronic transitions of Nd³⁺ ions in YAG centered around 800 and 880 nm, respectively. The grain pattern structure in the sample is again reproduced, showing a clear decrease in the total fluorescence intensity when approaching the GB. In particular, we observe an average intensity decrease of ~5 % with respect to the total fluorescence intensity when the emission spectra are recorded at the GBs. Similar images were obtained when the ${}^4F_{3/2} \rightarrow {}^4I_{11/2}$ electronic transition centered at 1060 nm was analyzed. Subtraction of the grain spectrum (~40 μm away from the GB) from the grain boundary spectrum reveals a clear structure at the shoulders of the main optical transition line

(Fig. 2B). Therefore, from Fig. 2B it can be inferred that the contribution of minor Nd^{3+} sites in YAG ceramics differs from grain to GBs. Similar peaks have been observed in samples of higher Nd^{3+} concentration, and have been labeled M_1 and M_2 spectral satellites [19-21]. It was found, that the M_1 satellite, corresponds to the first-order Nd^{3+} pairs (nearest-neighbor (NN)) while M_2 is connected with the second order (next-nearest-neighbor (NNN)) pairs, i.e. $\text{Nd}^{3+}(c)$ - $\text{Nd}^{3+}(c)$ pairs in the first and second coordination spheres. With increasing Nd^{3+} concentration, the relative intensities of these satellites increase while those of the isolated ions decrease due to concentration quenching processes activated by direct cross relaxation and migration-assisted energy transfer mechanisms inside the Nd^{3+} pairs. Figure 2C shows the confocal fluorescence image obtained when the contribution of the Nd^{3+} pairs to the total spectrum is analyzed. For such purpose, only the emission area in the satellite peaks, namely, M_1 center at 867.6 nm and/or M_2 center at 868.7 and 869.9 spectral regions were considered. A notable increase in the emitted satellite intensity is observed across grain boundaries, indicating a higher Nd^{3+} concentration at the grain boundaries. Details of the total emission area corresponding to M_1 - Nd^{3+} pairs and regular isolated Nd^{3+} ions when crossing a single GB is shown in Fig. 2D. A significant increase of $\sim 6\%$ in the contribution of M_1 pairs and a corresponding $\sim 4\%$ reduction in the regular isolated Nd^{3+} ions is observed across the GB. This is a clear indication of the increased Nd^{3+} concentration at the GBs, which leads to more pronounced Nd^{3+} segregation and increased Nd^{3+} - Nd^{3+} interaction.

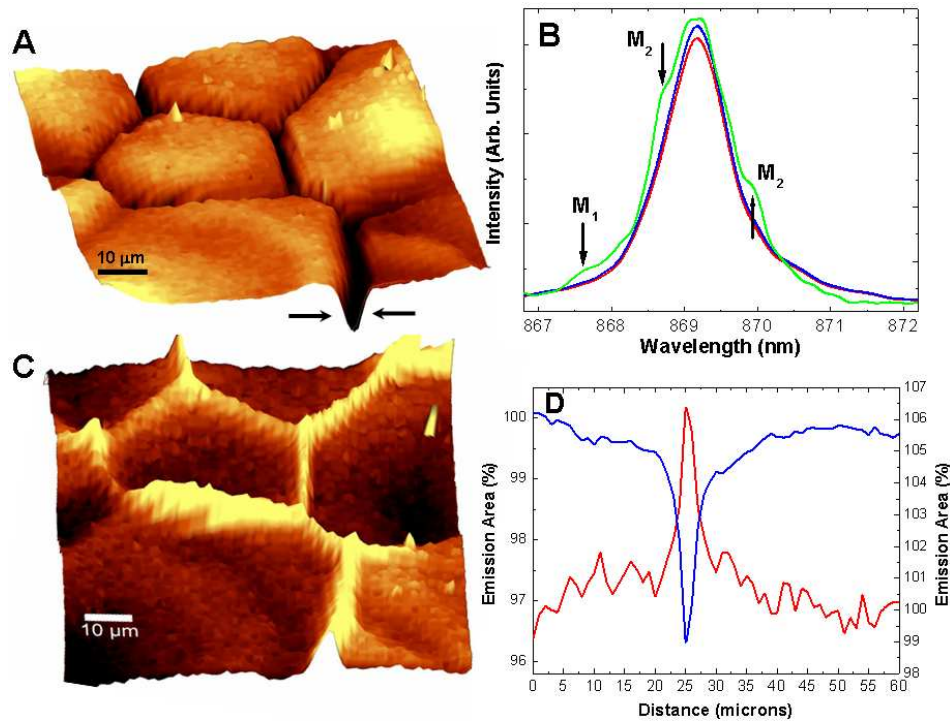


Fig. 2 (A) Three dimensional lateral fluorescence image (x - y scan; $85 \times 85 \mu\text{m}$) obtained in confocal geometry at a depth of $2 \mu\text{m}$ below the surface by integrating over the whole emission spectrum corresponding to the ${}^4\text{F}_{7/2}$ - ${}^4\text{S}_{3/2} \rightarrow {}^4\text{I}_{9/2}$ and ${}^4\text{F}_{3/2} \rightarrow {}^4\text{I}_{9/2}$ electronic transitions of Nd^{3+} ions YAG. The Nd^{3+} concentration was 1 at% (B) Green line: detail of the most intense line in the emission spectrum obtained subtracting the emission spectra from grains and GBs. For the illustration purposes, it has been multiplied by 20. Blue and red lines: emission spectra collected at grain and GB, respectively. (C) Confocal fluorescence image obtained when the contribution of the Nd^{3+} pairs to the total spectrum is analyzed. Note that only the emission area in the 867.7-868.5 nm (M_1 - Nd^{3+} pairs) and/or 869.8-870.6 (M_2 - Nd^{3+} pairs) spectral regions was considered. (D) Relative changes obtained in the total intensity of both, M_1 - Nd^{3+} pairs (red line, right y-axis) and regular isolated Nd^{3+} ions (blue line, left y-axis) when crossing a single grain boundary.

Thus, we can attribute the reduction in fluorescence quantum efficiency at the GBs to a more pronounced non-radiative decay channel. From measurements of the average quantum efficiency as a function of Nd^{3+} concentration, we can obtain a calibration curve for quantum efficiency versus concentration. Using it, we can conclude that the Nd^{3+} concentration is 0.1 at% higher at the GBs. This is also consistent with atomistic modeling studies in Nd^{3+} :YAG that predict a higher Nd^{3+} content was predicted at GBs [22]. Besides the decrease of emission quantum efficiency, the increased concentration and the resulting stronger correlation leads to an average decrease of $\sim 10\mu\text{s}$ (or $\sim 5\%$) in the fluorescence lifetime at the GBs in this 1 at% Nd^{3+} -doped sample, as estimated from a direct lifetime versus concentration measurement performed independently. Two main reasons can account for the observed Nd^{3+} segregation at GBs, namely solute drag effects due to the increased atomic mass and ionic radius of Nd^{3+} ion with respect to either Y^{3+} or Al^{3+} [23], and the influence of surface morphologies of grain boundaries on the relative concentration of Nd^{3+} ions in YAG [22]. Our results illustrate the exceptional sensitivity of our optical measurement technique. Concentration changes of this order were not detectable by other standard techniques such as Energy Dispersive Spectrometry (EDS), secondary ion mass spectroscopy (SIMS) and Electron Probe Microanalysis (EPMA).

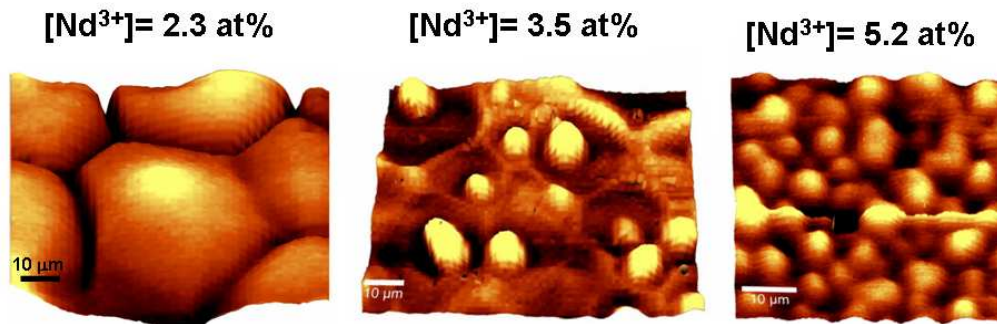


Figure 3 Three dimensional lateral fluorescence image (x - y scan; $85 \times 85 \mu\text{m}$) obtained in confocal geometry at a depth of $2 \mu\text{m}$ below the surface by integrating over the whole emission corresponding to the ${}^4\text{F}_{7/2}$: ${}^4\text{S}_{3/2} \rightarrow {}^4\text{I}_{9/2}$ and ${}^4\text{F}_{3/2} \rightarrow {}^4\text{I}_{9/2}$ electronic transitions of Nd^{3+} ions YAG for three different Nd^{3+} concentrations: 2.3 at% (left side), 3.5 at% (center) and 5.2 at% (right side).

Similar studies were performed on highly doped Nd^{3+} :YAG ceramics. Figure 3 shows the lateral confocal images obtained for different Nd^{3+} concentrations ranging from 2 at% up to 5.5 at%. Besides a decrease in the grain size with Nd^{3+} concentration as previously reported in other works [6], a gradual decrease in the optical quality was observed for Nd^{3+} concentrations exceeding 3 at%. Our studies show that not only is the Nd^{3+} segregation observed at the GBs, but also non-uniform dopant distribution within the grains ($\sim 2\%$ variation, or 0.07 at%, for the 3.5 at% sample and $\sim 4\%$ variation, or 0.21 at%, for the 5.2 at% sample) was observed in different areas in the sample. The yellow contrast regions observed in Fig. 3 indicate regions of higher Nd^{3+} content. A similar study of the commercial Konoshima Inc Nd^{3+} :YAG material with 4 at% doping reveals similar spatial inhomogeneities (0.7%, or an upper limit variation of 0.028 Nd^{3+} at%). Because of the efficient energy transfer process present in Nd^{3+} :YAG system, the observed spatial inhomogeneities in doping leads to locally enhanced energy transfer efficiencies among Nd^{3+} ions and may explain the observed laser instabilities. More specifically, we believe these spatial heterogeneities can act as saturable-absorber type defects as postulated in literature without direct evidence [8], that can explain the dynamical instabilities and the strong beam degradation observed in highly doped Nd^{3+} :YAG ceramics. Figure 4 shows a 3-dimensional spatial reconstruction of GBs in an 85

μm^3 volume obtained from the emission spectra of Nd^{3+} ions in YAG. Because self-fluorescence quenching across GB spreads over a couple of microns, nearly a quarter of the ceramic laser gain media ($\sim 20\%$ volume) presents additional optical losses.

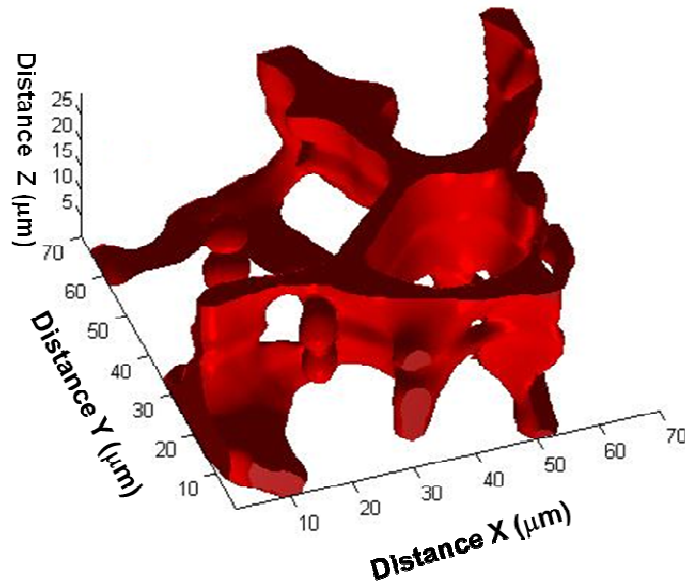


Fig. 4 Partially bottom view at a fixed elevation of the 3D isosurface spatial reconstruction of GB surfaces obtained from the whole emission spectra area of Nd^{3+} ions in YAG. Nd^{3+} concentration was 1 at%.

4. Summary and Conclusions

In summary, we have presented a non-invasive, sensitive and powerful method of 3D visualization of grains and grain boundaries in unetched transparent Nd^{3+} :YAG ceramics based on spatially resolved confocal spectroscopy. Our results show Nd^{3+} segregation and a decrease in the total fluorescence quantum efficiency of Nd^{3+} ions at GBs. Additionally, an increasingly non uniform Nd^{3+} distribution is found with Nd^{3+} doping level exceeding 3 at%. The observed Nd^{3+} segregation and spatial variations (0.1-0.2 at%) would give rise to spatial refractive index changes on the order of 10^{-5} on the grain scale [24], and hence, additional scattering losses, phase front distortions of the laser beam as well as slight perturbations of the TEM_{00} mode by populating higher order modes. For example, spatial index variations of 10^{-5} can lead to GHz shifts in laser tuning frequency over a 10cm rod length, which is 2-3 orders of magnitude higher than typical laser linewidths (MHz), thus leading to temporal instability [25,26]. This study indicates that grain sizes on the order of 1-2 microns are preferred for laser experiments since the microscopic dopant gradient due to GBs segregation ($\sim 2 \mu\text{m}$) is overcome. Interestingly, the commercial Konoshima Nd:YAG material, which has the highest laser performances reported, has a grain size smaller than $2 \mu\text{m}$, which would support the conclusion of this study. Though the study focuses on Nd^{3+} :YAG, the proposed study can be broadly applied to other ceramic laser materials.

Acknowledgments

We would like to acknowledge support from the Center for Optical Technologies at Pennsylvania State University, and VLOC Inc.